Astronomy & Astrophysics manuscript no. jetsufk
December 30, 2016
© ESO 2016

arXiv:1612.08890v1 [astro-ph.SR] 28 Dec 2016

Real light curves of FK Comae Berenices

L. Jetsu

Department of Physics, P.O. Box 64, FI-00014 University of Helsinki, Finland

Received / Accepted

ABSTRACT

Aims. To show that the observed light curves of FK Comae Berenices are interference of a nonstationary and a stationary light curve. These two "real" light curves follow the active longitude period ($P_{\rm act}$) and the rotation period ($P_{\rm rot}$) of FK Com.
Methods. The recently formulated general model for the light curves of chromospherically active binary stars is applied to 14 years of standard Johnson V photometry of FK Com.
Results. We determine a unique value, $P_{\rm rot} = 2.3976 \pm 0.0018$ days, for the rotation period of FK Com. The observed light curves can be modelled as interference of two real light curves, $f_1(\phi_{\rm act})$ and $f_2(\phi_{\rm rot})$, which are nonstationary and stationary in the rotational frame of reference. The observed "flip–flop" events, where the activity abruptly shifts 180 degrees in longitude, are connected to the interaction of these two curves at rotational phases $\phi_{\rm rot} = 0.0$ and 0.5.
Conclusions. Our light curve model can remove the "veil" of interference from the observed light curve, and give unique solutions for the real light curves $f_1(\phi_{\rm act})$ and $f_2(\phi_{\rm rot})$. The magnetic field evolution in chromospherically active single and binary stars is probably connected to the presence or absence of nonstationary and stationary parts in their observed light curves.

Key words. Methods: data analysis, Stars: activity, starspots, individual: FK Com

1. Introduction

Schwabe (1844) discovered the eleven years cycle in the number of sunspots in the Sun. Hale (1908) noticed the Zeeman effect caused by the solar magnetic field, and found out that this field is stronger in the sunspots. Kron (1947) made the first observations starspots in the light curves of eclipsing binaries. FK Comae Berenices (HD 117555, FK Com) was among the first late–type stars where starspots were discovered (Chugainov 1966). This chromosperically active single G4 giant (Strassmeier 2009) is the prototype of a class of variable stars, the FK Com class, defined by Bopp & Stencel (1981) as rapidly rotating single G–K giants. The members of this class could represent recently coalesced W UMa binaries (Webbink 1976). The starspots on the surface of FK Com concentrate on two long–lived active longitudes separated by 180 degrees, and undergo abrupt shifts between these longitudes (Jetsu et al. 1993). This "flip–flop" phenomenon has also been observed in chromospherically active binaries (e.g. Jetsu 1996, σ Gem). Numerous photometric studies of FK Com have been made (e.g. Korhonen et al. 2002; Oláh et al. 2006; Panov & Dimitrov 2007; Hackman et al. 2013).

Jetsu et al. (2016) presented a general model for the light curves of chromospherically active binary stars (hereafter CABS), and applied this model to the photometry of fourteen CABS. They also showed that the same model can be applied to the photometry of single stars, and studied one season of published photometry of FK Com. Here, we apply their model to the photometry of FK Com between the years 1996 and 2010.

2. Data

We study standard Johnson V photometry from Hackman et al. (2013). These data are summarized in Table 1. The observations were made with two telescopes, (Hackman et al. 2013, "T7" and "Ph10"), and were stored as two separate files into the CDS database. We analyse these two files separately, to avoid bias, as Hackman et al. (2013) also did. We do not study the first data segment in Hackman et al. (2013, SEG=1: $n = 24$), because it contains too few observations. The total number of observations in Table 1 is $n = 3844$.

Hackman et al. (2013) applied the continuous period search (hereafter CPS) method to this photometry. They determined 136 epochs of primary light curve minima ($t_{\rm min,1}$), but did not publish their numerical values. These epochs are given in our Table 2.

3. Methods

Jetsu et al. (2016) presented a general model for the light curves of CABS. This model has a nonstationary and stationary part. The active longitude period $P_{\rm act}$ determines the first nonstationary part

$$f_1(t, \bar{\beta}_1) = M_1 + \sum_{k=1}^{K_1} A_k \cos(\frac{2\pi kt}{P_{\rm act}}) + B_k \sin(\frac{2\pi kt}{P_{\rm act}}), \qquad (1)$$

where the order is $K_1 = 1$ or 2, and the free parameters are $\bar{\beta}_1 = [M_1, A_1, ..., A_{K_1}, B_1, ..., B_{K_1}]$. The orbital period $P_{\rm orb}$ determines the second stationary part

$$f_2(t, \bar{\beta}_2) = M_2 + \sum_{k=1}^{K_2} C_k \cos(\frac{2\pi kt}{P_{\rm orb}}) + D_k \sin(\frac{2\pi kt}{P_{\rm orb}}), \qquad (2)$$

where the order is $K_2 = 1$ or 2, and $\bar{\beta}_2 = [M_2, C_1, ..., C_{K_1}, D_1, ..., D_{K_1}]$ are the free parameters. The general light curve model (hereafter GLCM) combining these two parts is

$$f(t, \bar{\beta}) = f_1(t, \bar{\beta}_1) + f_2(t, \bar{\beta}_2), \quad (3)$$

where M_1 and M_2 are combined into one free parameter $M = M_1 + M_2$. The nonstationary $f_1(t, \bar{\beta}_1)$ and stationary $f_2(t, \bar{\beta}_2)$ parts of this linear model have a unique solution. We use the following two short notations "GLCM: $K_1 = 1, K_2 = 2$" and "GLCM: $K_1 = 2, K_2 = 2$" for the two different models applied in this paper. The K_1 and K_2 values are the orders used in Eqs. 1 and 2.

Jetsu et al. (2016) showed how GLCM can also be applied to the light curves of single stars by replacing $P_{\rm orb}$ with $P_{\rm rot}$ in Eq. 2. Here, we use the active longitude phases

$$\phi_{\rm act} = {\rm FRAC}[(t - t_{\rm act,0})/P_{\rm act}], \quad (4)$$

where $t_{\rm act,0} = 49877.321$ is the first epoch in Table 2, $P_{\rm act} = 2.401155$ days is the active longitude period (Hackman et al. 2013) and FRAC[x] removes the integer part of its argument x. The rotational phases are

$$\phi_{\rm rot} = {\rm FRAC}[(t - t_{\rm rot,0})/P_{\rm rot}], \quad (5)$$

where $P_{\rm rot} = 2.3976$ days (Sect. 4.1: Table 3) and $t_{\rm rot,0} = 50087.369$ (Sect. 4.2: Table 4).

Jetsu et al. (2016) applied GLCM to one seasonal light curve of FK Com. They tested $P_{\rm rot}$ values which were $\pm 15\%$ at both sides of the known $P_{\rm act} = 2.401155$ days value. The periodogram was

$$z_{\rm test}(P_{\rm rot}) = \sqrt{(1/n)\sum_i^n \epsilon_i^2}, \quad (6)$$

where ϵ_i are the GLCM residuals with the tested $P_{\rm rot}$. This test statistic is approximately the mean of the absolute values, $|\epsilon|$, of all residuals. Jetsu et al. (2016) subtracted a linear fit from the data before computing this periodogram. Here, we first compute the mean of all observations that are ± 30 days at both sides of each observation. Then we subtract this sliding mean from each observation, before computing $z_{\rm test}(P_{\rm rot})$ for tested periods $\pm 15\%$ at both sides of $P_{\rm act}$.

4. Results

4.1. Rotation period solution

The best rotation period for each segment is given in Table 3. We obtained the following mean $P_{\rm rot}$ estimates: 2.3966 ± 0.0020 days (GLCM: $K_1 = 1, K_2 = 2, n = 22$ values), 2.3985 ± 0.0031 days (GLCM: $K_1 = 2, K_2 = 2, n = 22$ values) and 2.3976 ± 0.0018 days (Both models, $n = 44$ values). The last value is used as $P_{\rm rot}$ of FK Com (Eqs. 2 and 5). Hackman et al. (2013) reported that the weighted mean of the observed photometric rotation period values $P_{\rm phot}$ was $P_{\rm w} = 2.3975 \pm 0.123$ days. This value is inaccurate, but equal to our $P_{\rm rot}$.

For example, the $P_{\rm rot}$ solution for the first segment of our photometry is shown in Fig. 1 (Ph10: SEG=1). The original data and the sliding mean are shown in Fig. 1a (crosses and continuous line). There are $n = 112$ observations during a time interval of about six months ($\Delta T =$ 180.6). The periodogram $z_{\rm test}$ of Eq. 6 shows one clearly defined minimum (Fig. 1b). The locations of best periods are denoted by the vertical continuous and dotted lines. They are practically the same for $K_1 = 1$ or 2 in Eq. 1. These best $P_{\rm rot}$ values given in Table 3 (Ph10, SEG=1) are 2.38692 days (GLCM: $K_1 = 1, K_2 = 2$) and 2.38724 days (GLCM: $K_1 = 2, K_2 = 2$). The two light curve models for the original data minus its sliding mean are shown in Figs. 1c. The continuous and dotted lines illustrating these models can not be separated from each other, because

Table 1. Standard Johnson V photometry. Telescope (Tel = T7 or Ph10), segments (SEG), first and last observing time (t_1 and t_n), time span and number of observations (ΔT and n)

Tel	SEG	t_1 HJD-2 400 000	t_n HJD-2 400 000	ΔT d	n
T7	1	50850.875	50997.687	146.8	224
T7	2	51153.047	51360.673	207.6	379
T7	3	51534.046	51706.736	172.7	68
T7	4	51883.044	52078.743	195.7	88
T7	5	52248.044	52461.698	213.7	220
T7	6	52614.048	52828.694	214.6	175
T7	7	52978.048	53185.717	207.7	131
T7	8	53343.046	53565.681	222.6	192
T7	9	53709.046	53922.698	213.7	194
T7	10	54075.045	54285.686	210.6	181
T7	11	54440.049	54643.730	203.7	187
T7	12	54807.040	55004.744	197.7	129
T7	13	55172.044	55297.831	125.8	111
Ph10	1	50085.055	50265.674	180.6	112
Ph10	2	50412.038	50636.678	224.6	209
Ph10	3	50778.042	50997.706	219.7	204
Ph10	4	51144.039	51362.728	218.7	179
Ph10	5	51508.043	51731.686	223.6	159
Ph10	6	51873.042	52089.727	216.7	193
Ph10	7	52242.033	52461.680	219.6	193
Ph10	8	52613.009	52826.679	213.7	159
Ph10	9	52972.029	53194.682	222.7	157

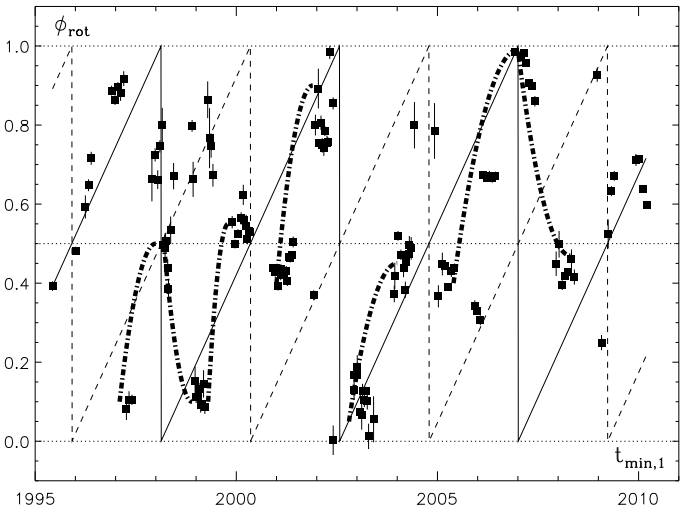

Fig. 3. Phases $\phi_{\rm rot}$ for primary minimum epochs of Table 2. Horizontal lines denote $\phi_{\rm rot} = 0.0$ and 0.5. Continuous and dashed zig-zag lines denote phases $\phi_{\rm act} = 0.0$ and 0.5, respectively. Thick dash dotted lines denote seven probable "flip–flop" events.

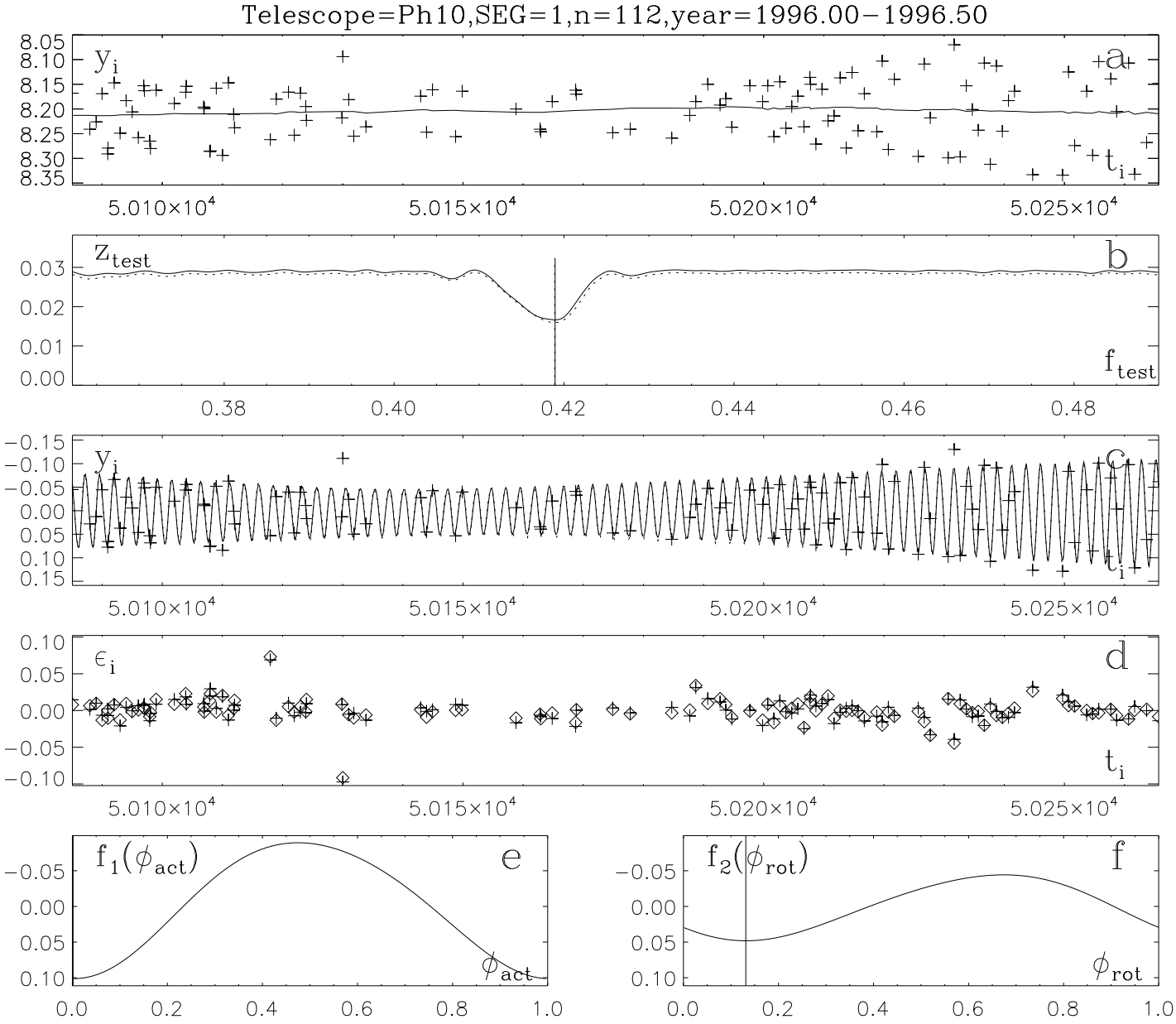

Fig. 1. Solutions of $P_{\rm rot}$ for Ph10: SEG =1. (a) Original data (crosses) and sliding mean (continuous line), (b) Periodograms of Eq. 6 (GLCM: $K_1 = 1, K_2 = 2$, continuous line, GLCM: $K_1 = 2, K_2 = 2$, dotted line) and locations of best periods (vertical continuous and dotted lines), (c) Data minus sliding mean (crosses), GLCM: $K_1 = 1, K_2 = 2$ (continuous line) and GLCM: $K_1 = 2, K_2 = 2$ (dotted line), (d) Residuals of GLCM: $K_1 = 1, K_2 = 2$ (crosses) and GLCM: $K_1 = 2, K_2 = 2$ (diamonds), (ef) $f_1(\phi_{\rm act})$ and $f_2(\phi_{\rm rot})$ of GLCM:$K_1 = 2, K_2 = 2$ (continuous lines). Vertical continuous line denotes primary minimum

the maximum difference between these two models is only $\Delta f = 0.^{\rm m}009$ (Table 3). The mean residuals of the models are $|\epsilon| = 0.^{\rm m}011$ (Fig. 1d: crosses) and $|\epsilon| = 0.^{\rm m}010$ (Fig. 1d: diamonds). This is a surprisingly good result, considering that we model six months of photometry ($n = 112$) of a chromospherically active star with seven ($K_1 = 1, K_2 = 2$) or nine ($K_1 = 2, K_2 = 2$) free parameters. Furthermore, it is known that optical flares occur FK Com (Jetsu et al. 1993). For example, there may be two such flares in Fig. 1c. In the former studies of FK Comae class stars, e.g. in Jetsu et al. (1999, V1794 Cyg) or Hackman et al. (2013, FK Com), it has been possible to model about 30 days of photometry with six free parameters. After this time interval, these models could not follow the changes of the amplitude and the shape of the light curve.

The solutions for the nonstationary part $f_1(\phi_{\rm act})$ and stationary part $f_2(\phi_{\rm rot})$ are shown in Fig. 1ef. The nonstationary part dominates, because it has a higher amplitude than the stationary part. Both light curves have only one minimum.

4.2. Nonstationary and stationary light curves

All seasonal light curves of the nonstationary and stationary part are shown in Fig. 2. The numerical values for the parameters of these curves are given Table 4. The max-

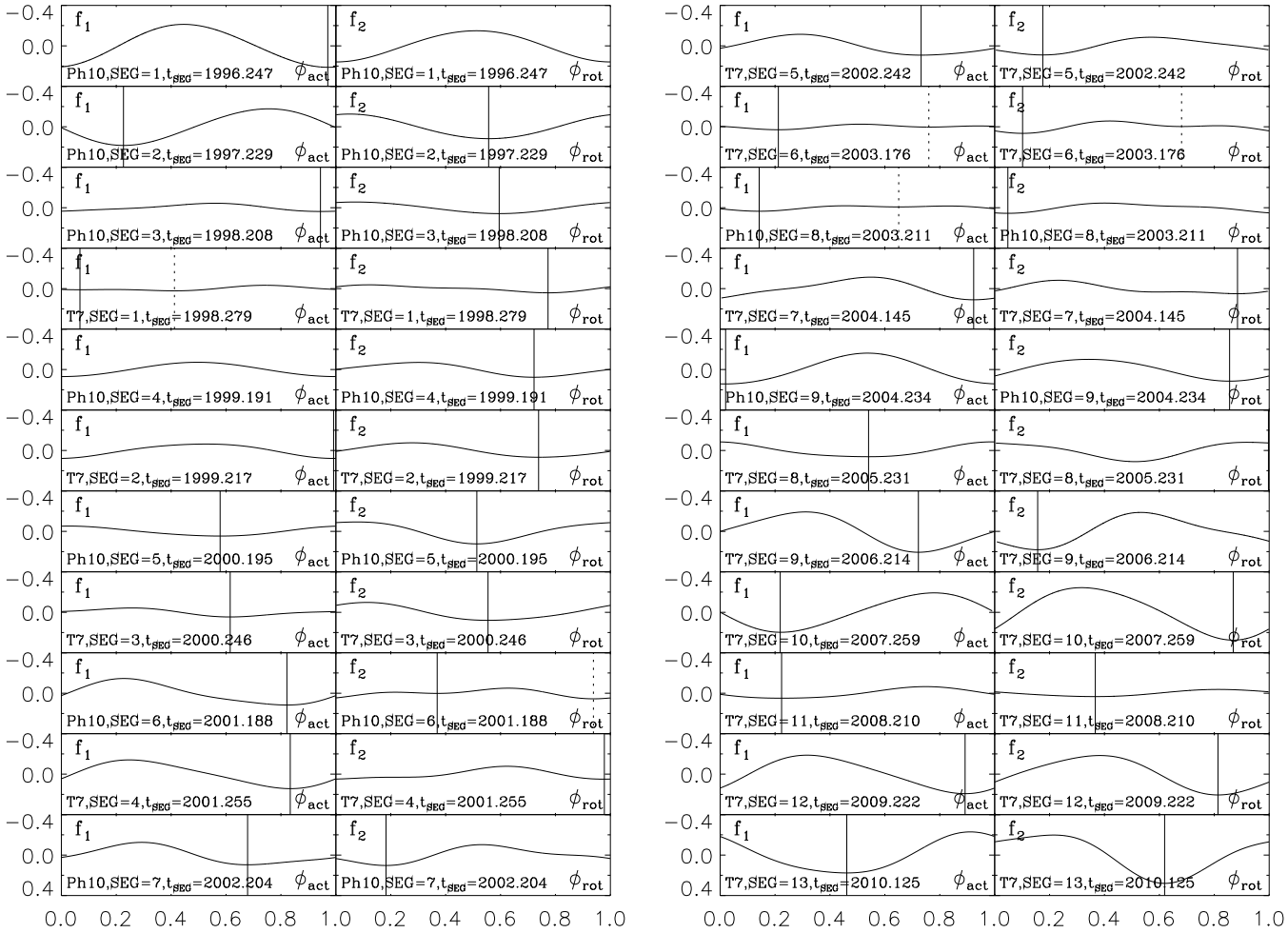

Fig. 2. Seasonal nonstationary and stationary light curves $f_1(\phi_{\rm act})$ and $f_2(\phi_{\rm rot})$ of FK Com. Vertical continuous and dotted lines show locations of primary and secondary (if present) minima. Numerical parameters of these light curves are given in Table 4.

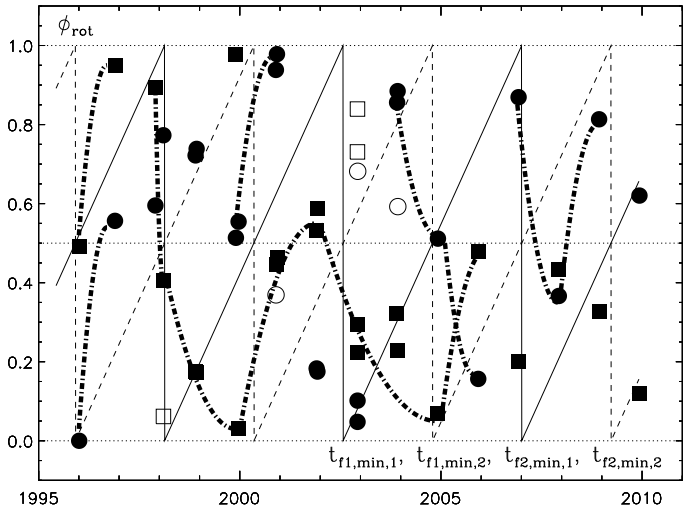

Fig. 4. Phases $\phi_{\rm rot}$ for light curve minima of Table 4. Parameters are $t_{\rm f1,min,1}$ (closed squares), $t_{\rm f1,min,2}$ (open squares), $t_{\rm f2,min,1}$ (closed circles) and $t_{\rm f2,min,2}$ (open circles). First closed circle on the left is the zero epoch of Eq. 5. (Table 4: bold value). All lines and probable "flip–flop" events are marked as in Fig. 3.

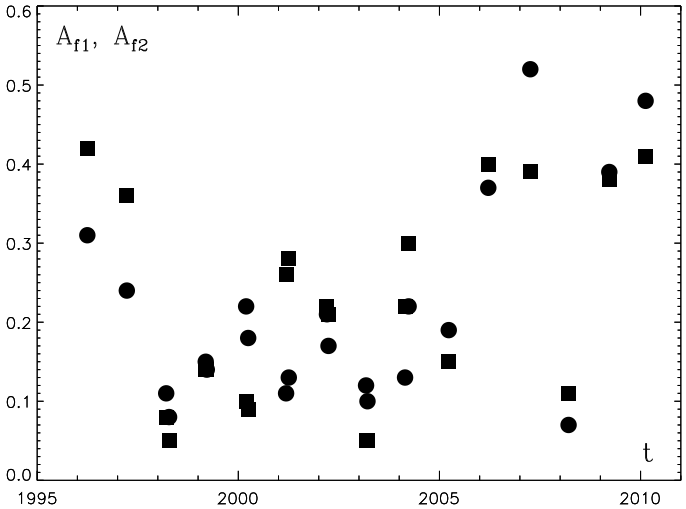

Fig. 5. Variations of $A_{\rm f1}$ (closed squares) and $A_{\rm f2}$ (closed circles).

imum peak to peak amplitude of $f_1(\phi_{\rm act})$ is $A_{\rm f1} = 0.^{\rm m}42$, while that of of $f_2(\phi_{\rm rot})$ is even higher, $A_{\rm f2} = 0.^{\rm m}52$. Both parts are sometimes very weak, e.g. in the years 1998 and

Table 2. Primary minimum epochs ($t_{\rm min,1}$) from Hackman et al. (2013, $n = 136$). Epoch $t_{0,\rm act}$ of Eq. 4 is marked in bold.

$t_{\rm min,1}$ HJD-2400000	$t_{\rm min,1}$ HJD-2400000	$t_{\rm min,1}$ HJD-2400000
49877.321 ± 0.029	51642.241 ± 0.033	53080.493 ± 0.049
50086.126 ± 0.025	51659.075 ± 0.043	53087.851 ± 0.044
50175.104 ± 0.070	51668.658 ± 0.024	53109.483 ± 0.032
50204.007 ± 0.036	51874.631 ± 0.022	53116.728 ± 0.055
50228.146 ± 0.040	51898.584 ± 0.029	53133.491 ± 0.069
50413.172 ± 0.029	51924.874 ± 0.029	53163.009 ± 0.141
50444.283 ± 0.029	51948.913 ± 0.030	53345.192 ± 0.169
50470.739 ± 0.027	51951.351 ± 0.026	53380.153 ± 0.067
50494.677 ± 0.049	51972.901 ± 0.021	53416.313 ± 0.069
50523.534 ± 0.045	51977.689 ± 0.012	53442.675 ± 0.019
50547.902 ± 0.065	51999.291 ± 0.029	53468.922 ± 0.014
50571.937 ± 0.051	52008.821 ± 0.033	53497.790 ± 0.037
50598.309 ± 0.031	52025.749 ± 0.032	53526.579 ± 0.026
50779.470 ± 0.137	52035.333 ± 0.028	53710.965 ± 0.033
50808.386 ± 0.040	52052.134 ± 0.021	53734.906 ± 0.021
50832.212 ± 0.057	52061.803 ± 0.033	53761.226 ± 0.030
50851.594 ± 0.037	52248.492 ± 0.030	53788.482 ± 0.015
50873.301 ± 0.106	52263.910 ± 0.063	53817.234 ± 0.024
50877.370 ± 0.033	52290.505 ± 0.121	53843.621 ± 0.029
50898.929 ± 0.091	52297.368 ± 0.013	53869.980 ± 0.027
50903.766 ± 0.040	52314.274 ± 0.043	53898.767 ± 0.024
50922.786 ± 0.051	52326.124 ± 0.043	54076.940 ± 0.016
50929.852 ± 0.060	52340.495 ± 0.049	54129.655 ± 0.023
50949.387 ± 0.084	52350.187 ± 0.030	54153.655 ± 0.022
50976.089 ± 0.080	52369.298 ± 0.043	54179.967 ± 0.018
51144.226 ± 0.036	52376.496 ± 0.029	54203.825 ± 0.021
51153.492 ± 0.106	52393.821 ± 0.040	54227.783 ± 0.017
51171.450 ± 0.086	52424.681 ± 0.037	54256.460 ± 0.032
51180.946 ± 0.039	52425.035 ± 0.089	54449.680 ± 0.074
51195.327 ± 0.047	52614.750 ± 0.059	54476.172 ± 0.081
51207.368 ± 0.035	52614.842 ± 0.031	54504.695 ± 0.030
51221.655 ± 0.047	52641.215 ± 0.036	54531.123 ± 0.017
51233.650 ± 0.017	52643.661 ± 0.072	54555.126 ± 0.013
51248.155 ± 0.083	52664.968 ± 0.018	54588.768 ± 0.060
51260.001 ± 0.040	52684.128 ± 0.088	54615.034 ± 0.046
51285.843 ± 0.112	52691.467 ± 0.044	54822.453 ± 0.042
51302.393 ± 0.182	52708.194 ± 0.041	54861.589 ± 0.046
51316.734 ± 0.074	52720.240 ± 0.024	54922.188 ± 0.088
51333.337 ± 0.069	52734.564 ± 0.052	54951.219 ± 0.030
51508.077 ± 0.037	52746.337 ± 0.077	54977.685 ± 0.029
51534.318 ± 0.026	52791.995 ± 0.140	55174.385 ± 0.036
51560.755 ± 0.027	52979.768 ± 0.050	55198.365 ± 0.024
51589.618 ± 0.038	52984.673 ± 0.080	55238.946 ± 0.017
51608.942 ± 0.061	53013.687 ± 0.029	55270.018 ± 0.016
51615.982 ± 0.036	53039.946 ± 0.032	
51635.129 ± 0.066	53063.843 ± 0.057	

Table 3. Rotation periods $P_{\rm rot}$ determined with $z_{\rm test}$ (Eq. 6). GLCM: $K_1 = 1$ and K_2 period and mean residual ($P_{\rm rot}$ and $|\epsilon|$), same for GLCM: $K_1 = 2$ and K_2, maximum difference between these two models (Δf)

		GLCM $K_1 = 1, K_2 = 2$		GLCM $K_1 = 2, K_2 = 2$		
Tel	SEG	$P_{\rm rot}$ d	$\lvert\epsilon\rvert$ mag	$P_{\rm rot}$ d	$\lvert\epsilon\rvert$ mag	Δf mag
T7	1	2.39900	0.009	2.43844	0.009	0.020
T7	2	2.40139	0.011	2.38292	0.011	0.040
T7	3	2.40051	0.012	2.41393	0.012	0.026
T7	4	2.39970	0.012	2.39852	0.011	0.019
T7	5	2.39083	0.015	2.39244	0.015	0.007
T7	6	2.39258	0.010	2.39072	0.009	0.016
T7	7	2.42077	0.013	2.42360	0.012	0.016
T7	8	2.38889	0.012	2.38760	0.011	0.013
T7	9	2.39137	0.011	2.39110	0.011	0.002
T7	10	2.39548	0.010	2.39794	0.009	0.020
T7	11	2.37800	0.015	2.37662	0.014	0.010
T7	12	2.40933	0.015	2.40787	0.014	0.022
T7	13	2.39352	0.006	2.39261	0.006	0.005
Ph10	1	2.38692	0.011	2.38724	0.010	0.009
Ph10	2	2.40225	0.013	2.40148	0.013	0.004
Ph10	3	2.40411	0.010	2.40991	0.010	0.014
Ph10	4	2.39614	0.013	2.38412	0.012	0.032
Ph10	5	2.39880	0.014	2.40836	0.012	0.029
Ph10	6	2.38531	0.013	2.38662	0.012	0.013
Ph10	7	2.39100	0.016	2.39595	0.015	0.030
Ph10	8	2.39032	0.015	2.38925	0.015	0.015
Ph10	9	2.40829	0.025	2.41064	0.025	0.019

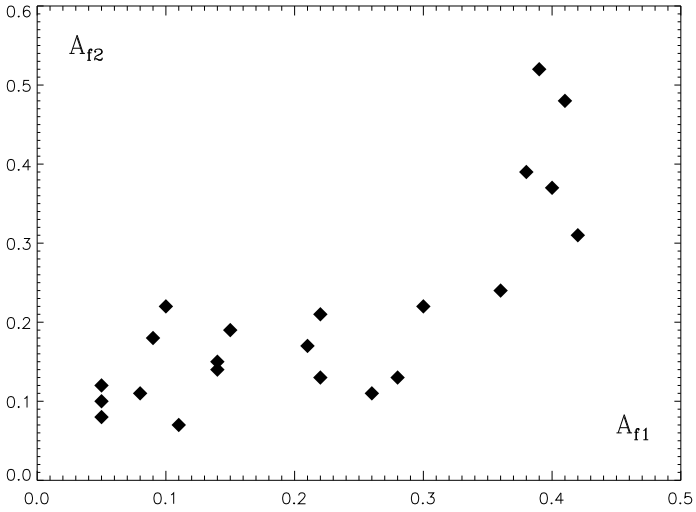

Fig. 6. Correlation of $A_{\rm f1}$ and $A_{\rm f2}$

2003. In only a few cases, do these light curves have two minima, e.g. in the years 1998 or 2003 when their amplitudes are low. Our models for the temporally overlapping data from different telescopes are consistent.

We emphasize that there is no unique phase for presenting the observed light curves, like for example with the TSPA method (e.g. Jetsu & Pelt 1999) or the CPS method (e.g. Lehtinen et al. 2011). In the GLCM approach, the observed light curves are changing at every moment in time and can be studied only as a function of time, not as a function of phase. The only unique phases are the phases of the nonstationary and stationary part of the light curve (Eqs. 4 and 5). These curves $f_1(\phi_{\rm act})$ and $f_2(\phi_{\rm rot})$ are the "real" light curves of FK Com. The observed light curves represent the interference of these two curves. In other words, our Fig. 2 displays the real light curves "behind" the observed light curves.

4.3. Observed light curve minima

The phases of $f_1(\phi_{\rm act})$ and $f_2(\phi_{\rm rot})$ curves coincide once in a lap cycle of $P_{\rm cyc} = |[P_{\rm rot}^{-1} - P_{\rm act}^{-1}]^{-1}|$ (Jetsu et al. 2016, their Eq. 4). FK Com has $P_{\rm cyc} = 4.43$ years.

The rotational phases $\phi_{\rm rot}$ (Eq. 5) for the light curve minima $t_{\rm min,1}$ of Table 2 are shown in Fig. 3. The zero epoch for the active longitude phases $\phi_{\rm act}$ (Eq. 4) is fixed

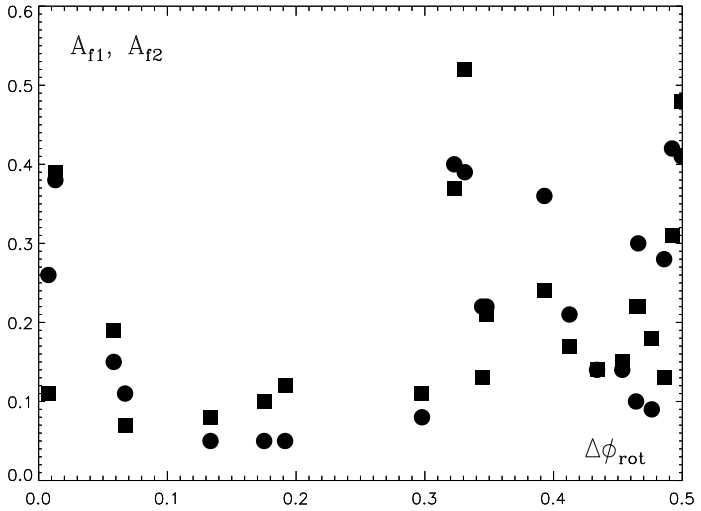

Fig. 7. A_{f1} and A_{f2} versus orbital phase difference $\Delta\phi_{orb}$ of $f_1(\phi_{act})$ and $f_2(\phi_{rot})$ light curve primary minima.

to the first light curve minimum epoch (Fig. 3: first closed rectangle on the left). The migrating zig-zag lines $\phi_{act} = 0.0$ (continuous line) and $\phi_{act} = 0.5$ (dashed line) are unambiguous in the rotational frame of reference. The light curve minima show a tendency to concentrate either on these zig-zag lines, or to rotational phases $\phi_{rot} \approx 0.0$ and 0.5 (Fig. 3: horizontal dotted lines). We have outlined seven probable "flip–flop" events (Fig. 3: thick curved dashed dotted lines). These events usually begin and end close to the phases $\phi_{rot} \approx 0.0$ and 0.5.

4.4. Nonstationary and stationary light curve minima

The rotational phases ϕ_{rot} of the primary and secondary minima of the nonstationary and stationary seasonal light curves from Table 4 are shown in Fig. 4. Many of the minima of the stationary part $f_2(\phi_{rot})$ stay close to $\phi_{rot} \approx 0.0$ and 0.5 (Fig. 4: closed circles). Numerous phase shifts can be interpreted as "flip–flop" events (Fig. 4: thick curved dash dotted lines). The primary minima $t_{min,1}$ of the observed light curves are determined by the interference of the $f_1(\phi_{act})$ and $f_2(\phi_{rot})$ curves. For example, these "real" light curves show a clear "flip–flop" between 1995 and 1996 (Fig. 4). This event is not seen at all in the observed light curves (Fig. 3). The "flip–flop" events tend to begin and end close to $\phi_{rot} \approx 0.0$ and 0.5 in Fig. 4, just like in Fig. 3.

4.5. Nonstationary and stationary light curve amplitudes

The seasonal changes of the $f_1(\phi_{act})$ and $f_2(\phi_{rot})$ light curve amplitudes are shown in Fig. 5. Except for the dip in the year 2008, these A_{f1} and A_{f2} changes are quite regular. They even show some correlation with the observed changes of the mean brightness of FK Com (see Hackman et al. 2013, their Fig. 1). The changes of A_{f1} and A_{f2} are clearly correlated in time (Fig. 6). Finally, the largest scatter in these amplitudes occurs when the separation of the minima of $f_1(\phi_{act})$ and $f_2(\phi_{rot})$ light curves is $\Delta\phi_{rot} = 0.0$ or 0.5 (Fig. 7). All results in Figs. 3–7 support the idea that something happens when the minimum of $f_1(\phi_{act})$ curve crosses the rotational phases $\phi_{rot} = 0.0$ or 0.5, i.e. the minima of the $f_2(\phi_{rot})$ curve. The interference of the two light curves is strongest at these phases. The opposite is true for $\Delta\phi_{rot} = 0.25$, i.e. the amplitudes A_{f1} and A_{f2} are small, and their scatter is small (Fig. 7). These regularities are similar to those discovered by Jetsu et al. (2016) in the photometry of fourteen CABS which was also analysed with GLCM.

4.6. Detectability of stationary light curve period P_{rot}

Here, we illustrate how the period of the nonstationary light curve $f_2(\phi_{rot})$ can, or can not, be detected. The non-weighted Kuiper test periodogram V_n (Jetsu & Pelt 1996, their Eq. 18) for light minima of Table 2 is shown in Fig. 8a for the period range ±15 % at both sides P_{act}. The highest peak coincides with $P_{act} = 2.401151$ days. However, there is no such high peak at $P_{rot} = 2.3976$ days. The magnified periodogram close to P_{act} is shown in Fig. 8b. The sixth and seventh best values P_6 and P_7 are close to $P_{rot} = 2.3976 \pm 0.0018$ days. The peaks of P_2, P_3, P_4 and P_5 are spurious (i.e. unreal) periods connected to $P_1 = P_{act}$, because their round differences with P_{act} are integers during the whole time span of data (Fig. 8b: compare R values).

The power spectrum z_{LS} (Scargle 1982) for all T7 photometry is shown in Fig. 8c. The tested period range is the same as in Fig. 8a. The magnified periodogram shows that the best period, $P_1 = 2.4016$ days is close, but not exactly equal, to P_{act}. However, the z_{LS} power spectrum shows no traces of P_{rot} (Fig. 8d).

Finally, we tested, if the pilot search method formulated by Jetsu & Pelt (1999, their Eq. 3: Θ_{pilot}) would detect P_{rot} from the T7 photometry. This method can adapt to period changes and phase shifts, because it correlates only pairs of observations closer than $D_{max} = Q_{pilot} \times P_{max}$ in time. We tested values $Q_{pilot} = 10$, 50 and 100 with $P_{max} = 2.75$, but found no traces of P_{rot} in the Θ_{pilot} periodogram (Fig. 8e).

Jetsu et al. (2016) first detected traces of the stationary part in the light curves of fourteen CABS from the binned mean light curves (hereafter MLC). All photometry of FK Com made with the T7 telescope is shown in Fig. 9a. The binned light curve with $P_{rot} = 2.3976$ days and 20 bins with a width of $\Delta\phi = 0.05$ in phase is shown in Fig. 9b. This is the MLC of FK Com. Traces of the stationary light curve $f_2(\phi_{rot})$ of FK Com can be detected in MLC, just like such traces were detected in the MLC of the above mentioned fourteen CABS. We emphasize that this P_{rot} periodicity was already detected from the z_{test} periodograms (Eq. 6) of different seasons (Sect. 4.1: Table 3 and Fig. 1).

5. Discussion

The value of the rotation period P_{rot} is a free parameter only in the analysis of Sect. 4.1. This analysis gives the fixed $P_{rot} = 2.3976$ days value used in all subsequent analysis. For example, the $f_1(\phi_{act})$ and $f_2\phi_{rot})$ curves in Figs. 1ef are slightly different from those in Fig. 2 (Ph10: SEG=1), because the P_{rot} value was 2.38724 days in the former figure, and 2.3976 days in the latter figure. Our analysis with the fixed value of $P_{rot} = 2.3976$ days is unambiguous. Additional photometry will certainly provide a more accurate P_{rot} estimate, but the locations of active longitudes can be unambiguously determined in the current, or in any new revised, rotational frame of reference. It is also essential to understand the difference between the phases of Eqs. 4 and

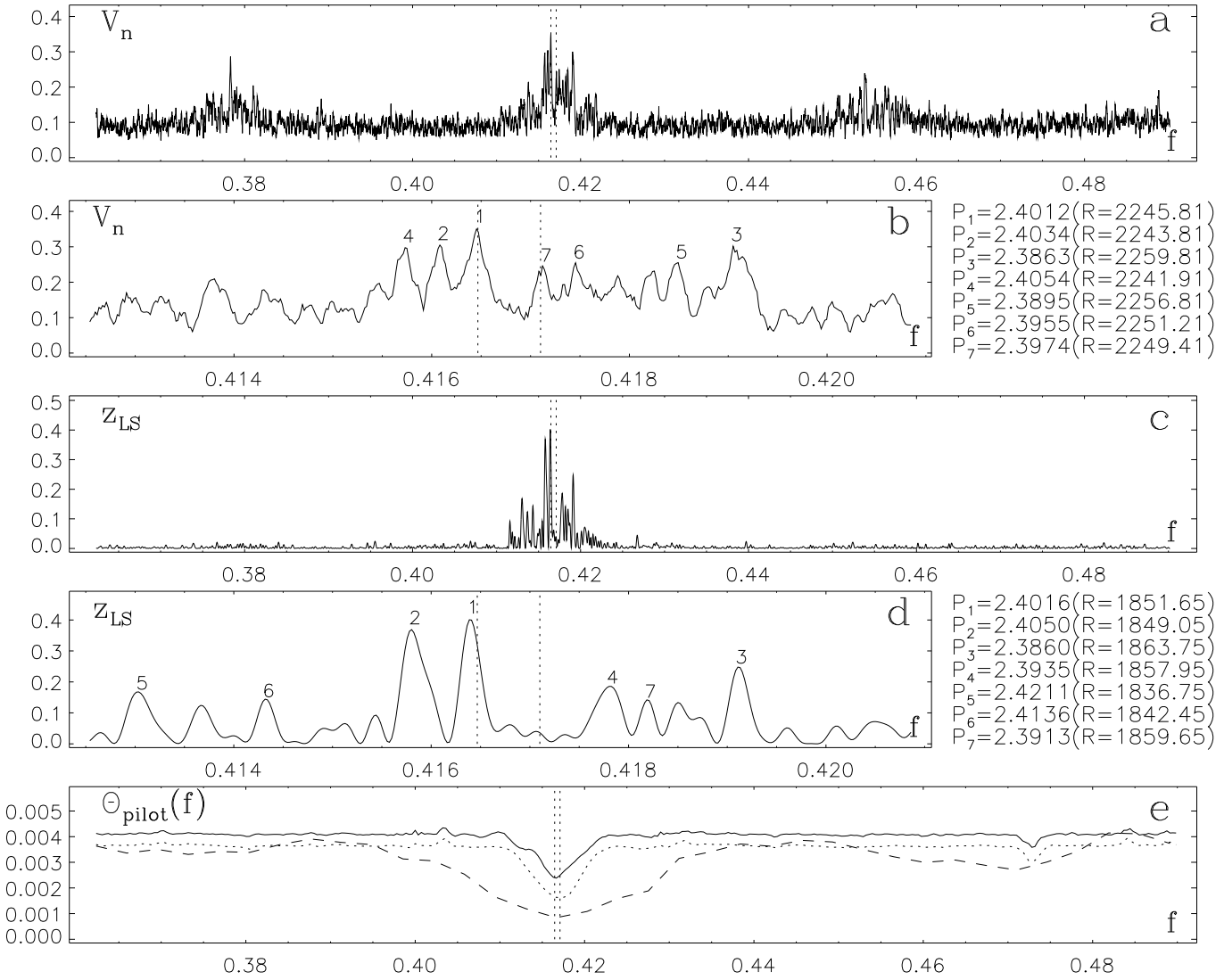

Fig. 8. (a) Kuiper periodogram V_n (continuous line) for primary minima of Table 2. Locations of $P_{\rm act}$ and $P_{\rm rot}$ (dotted vertical lines). (b) Magnified V_n periodogram close to $P_{\rm act}$. Values of seven best periods are given on the right, and number of round completed (R) during the time span of data, $\Delta T = 5393$ days. (c) Power spectrum $z_{\rm LS}$ for telescope T7 photometry. Vertical dotted lines as in "a". (d) Magnified power spectrum close to $P_{\rm act}$. Values of seven best periods are given on the right, and number of round completed (R) during the time span of data, $\Delta T = 4447$ days. Vertical lines as in "b". (e) Pilot search periodogram $\Theta_{\rm pilot}$ for telescope T7 photometry computed with $D_{\rm max} = Q_{\rm pilot} \times P_{\rm max}$, where $P_{\rm max} = 2.75$ and $Q_{\rm pilot} = 10$ (dashed line). 50 (dotted line) and 100 (continuous line). Vertical dotted lines as in "a".

5, i.e. the connection between to the $P_{\rm act}$ and $P_{\rm rot}$ frames of reference. For example, the f_1 curve primary minimum epoch $t_{\rm f1,min,1}$ phases $\phi_{\rm act,f1,min1}$ are computed from Eq. 4 in Table 4. However, the phases of the same epochs $t_{\rm f1,min,1}$ are computed from Eq. 5 in Fig. 4. The chosen zero epochs in Eqs. 4 and 5 represent the moments in time when the spots connected to the nonstationary and stationary parts for the first time crossed the centre of the visible stellar disk of FK Com.

The nonstationary and stationary light curves, $f_1(\phi_{\rm act})$ and $f_2(\phi_{\rm rot})$, are the "real" light curves of FK Comae (Fig. 2). The observed light curve is a result of their interference. These $f_1(\phi_{\rm act})$ and $f_2(\phi_{\rm rot})$ curves are mostly single peaked, but can be double peaked when their amplitudes are low. The maximum amplitude values in Table 4, $A_{\rm f1} = 0.^{\rm m}42$ and $A_{\rm f2} = 0.^{\rm m}52$, indicate that the observed maximum amplitude of the light curve of FK Com could reach $0.^{\rm m}9$. Here, we study only the seasonal means of the $f_1(\phi_{\rm act})$ and $f_2(\phi_{\rm rot})$ curves. It is evident that they are both changing also within the seasons. However, a more detailed analysis of those changes is not pursued in the current study.

Numerous "flip–flop" events were identified from the minima of the observed light curves (Fig. 3), as well as from the minima of the $f_1(\phi_{\rm act})$ and $f_2(\phi_{\rm rot})$ curves (Fig. 4). These events show a tendency to begin and end at the rotational phases $\phi_{\rm rot} = 0.0$ and 0.5. The changes of $f_1(\phi_{\rm act})$ and $f_2(\phi_{\rm rot})$ amplitudes are quite regular in time (Fig. 5), and they are also strongly correlated (Fig. 6). There may be a reasonable explanation for the sudden dip that occurs in the year 2008 (Fig. 5). The $f_1(\phi_{\rm act})$ and $f_2(\phi_{\rm rot})$ curves can cancel each other out even when their amplitudes are very high. In that case, the observed light curve is

Table 4. Seasonal GLCM: $K_1 = 2$, $K_2 = 2$ results. Telescope (T7 or Ph10), segment (SEG), mean of all observing times ($t_{\rm SEG}$), mean residual ($|\epsilon|$), amplitude of f_1 curve (A_{f_1}), primary and secondary minimum epochs and phases of f_1 curve ($t_{f_1,min,1}$,$\phi_{act,f_1,min,1}$, $t_{f_1,min,2}$,$\phi_{act,f_1,min,2}$), amplitude of f_2 curve (A_{f_2}), primary and secondary minimum epochs and phases of f_2 curve ($t_{f_2,min,1}$,$\phi_{rot,f_2,min,1}$, $t_{f_2,min,2}$,$\phi_{rot,f_2,min,2}$). Epoch $t_{0,\rm rot}$ of Eq. 5 is marked in bold in column $t_{f_2,min,1}$.

Tel	SEG	$t_{\rm SEG}$	$\|\epsilon\|$	A_{f_1}	$t_{f_1,min,1}$	$\phi_{act,f_1,min,1}$	$t_{f_1,min,2}$	$\phi_{act,f_1,min,2}$	A_{f_2}	$t_{f_2,min,1}$	$\phi_{rot,f_2,min,1}$	$t_{f_2,min,2}$	ϕ_{rot}
		y	mag	mag	HJD		HJD		mag	HJD		HJD	
T7	1	1998.279	0.009	0.05	50853.178	0.41	50852.351	0.07	0.08	50851.659	0.77		
T7	2	1999.217	0.011	0.14	51154.714	0.99			0.14	51153.674	0.74		
T7	3	2000.246	0.012	0.09	51535.593	0.62			0.18	51534.451	0.55		
T7	4	2001.255	0.011	0.28	51884.284	0.83			0.13	51883.119	0.98		
T7	5	2002.242	0.015	0.21	52249.015	0.73			0.17	52250.424	0.17		
T7	6	2003.176	0.010	0.05	52615.142	0.21	52614.054	0.76	0.12	52614.683	0.10	52616.074	
T7	7	2004.145	0.014	0.22	52979.424	0.92			0.13	52978.598	0.88	52980.295	
T7	8	2005.231	0.013	0.15	53343.477	0.54			0.19	53344.536	0.51		
T7	9	2006.214	0.012	0.40	53711.292	0.72			0.37	53710.518	0.15		
T7	10	2007.259	0.009	0.39	54075.058	0.22			0.52	54076.662	0.87		
T7	11	2008.210	0.020	0.11	54442.450	0.23			0.07	54442.289	0.36		
T7	12	2009.222	0.015	0.38	54809.026	0.89			0.39	54807.796	0.81		
T7	13	2010.125	0.007	0.41	55172.966	0.46			0.48	55174.166	0.62		
Ph10	1	1996.247	0.012	0.42	50086.151	0.97			0.31	**50087.369**	1.00		
Ph10	2	1997.229	0.013	0.36	50413.321	0.23			0.24	50412.379	0.55		
Ph10	3	1998.208	0.010	0.08	50780.019	0.94			0.11	50779.305	0.59		
Ph10	4	1999.191	0.013	0.14	51145.131	0.00			0.15	51144.044	0.72		
Ph10	5	2000.195	0.014	0.10	51509.092	0.58			0.22	51510.377	0.51		
Ph10	6	2001.188	0.013	0.26	51874.650	0.82			0.11	51873.433	0.94	51874.466	
Ph10	7	2002.204	0.015	0.22	52244.084	0.68			0.21	52243.250	0.18		
Ph10	8	2003.211	0.015	0.05	52614.974	0.14	52613.794	0.65	0.10	52614.554	0.05		
Ph10	9	2004.234	0.027	0.30	52972.453	0.02			0.22	52973.734	0.85		

nearly constant, and when the observational error $0.^{\rm m}006$ is superimposed on this observed nearly constant brightness, it may not be possible to retrieve the original real amplitudes $A_{\rm f1}$ and $A_{\rm f2}$. The idea of interference also explains why the scatter of these amplitudes is largest at phases $\phi_{\rm rot} = 0.0$ and 0.5 (Fig. 7), where the "flip–flop" events tend to begin and end (Figs. 3 and 4). We do not claim that this regularity fully explains the "flip–flop" events, but it does provide one new constraint to understand them better. All these regularities indicate that GLCM describes real physical phenomena that cause the light curve of FK Com. The simple assumption that active longitudes ($P_{\rm act}$) and rotation ($P_{\rm rot}$) determine the light curves of FK Com, allows GLCM to discover all the above mentioned regularities in the $f_1(\phi_{\rm act})$ and $f_2(\phi_{\rm rot})$ light curves. These two light curves could certainly be signatures of longitudinally nonstationary and stationary magnetic fields (Jetsu et al. 2016).

A unique $P_{\rm rot}$ value can be determined by applying the periodogram of Eq. 6 to the photometry of FK Com. However, the Kuiper test can not detect this $P_{\rm rot}$ periodicity from the light curve minima (Fig. 8ab). Nor could it be detected from the original FK Com photometry (Fig. 8cde) with power spectrum method (Scargle 1982) or the pilot search method (Jetsu & Pelt 1999). Traces of this periodicity are present in MLC of FK Com (Fig. 9).

The analysis presented here for FK Com, and that of fourteen CABS in Jetsu et al. (2016), shows that GLCM can be successfully applied to the light curves of binary and single chromospherically active stars. The model of Eq. 3 can probably be applied to the light curves of any single chromospherically active star (e.g. Lehtinen et al. 2012, LQ Hya). The latest 3rd version of CABS catalogue (Eker et al. 2008) lists the numerous different observed values for the variable photometric rotation periods $P_{\rm phot}$ of each binary star. Our GLCM analysis suggest that these $P_{\rm phot}$ values can be replaced by a single unambiguous $P_{\rm rot}$ value. Thus, the next updated catalogue could contain both binary and single chromospherically active stars. Furthermore, many binaries in the current 3rd catalogue version already have $P_{\rm rot} = P_{\rm orb}$, because their orbital and rotational motion is synchronized. FK Com probably "inherited" $P_{\rm rot} = P_{\rm orb}$ in the coalescence of two stars (Bopp & Stencel 1981). Our analysis shows that the chromospherically active binary stars (CABS) and single stars are simply chromospherically active stars (CAS), at least in the case of light curve analysis.

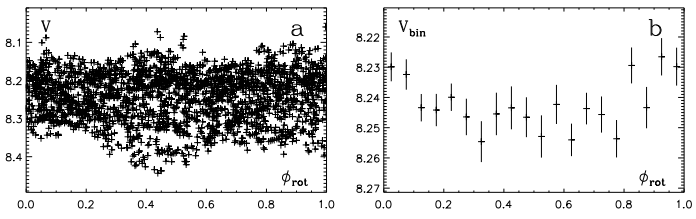

Fig. 9. (a) All V magnitude data of T7 telescope photometry, (b) Binned magnitudes $V_{\rm bin}$

The results presented here, and in Jetsu et al. (2016), reveal several regularities in the temporal evolution of magnetic fields in chromospherically active single and binary stars. We propose that as the rotation of these stars slows down, their magnetic field evolution proceeds through four observable stages

1. The magnetic field has non-axisymmetric *longitudinally* nonstationary and stationary parts. Both can be de-

tected from the light curve. This is observed here in FK Com or in the fourteen CABS studied by Jetsu et al. (2016).
2. The magnetic field has a non-axisymmetric *longitudinally* stationary part which can be detected from the light curve. The nonstationary part (active longitudes) is weak or absent (e.g. Lehtinen et al. 2016, Fig. 14, right panel: dividing line).
3. The magnetic field has only an axisymmetric part. This part can be *latitudinally* stationary (e.g. Strassmeier & Rice 1998, EK Dra: polar spot) or nonstationary (e.g. the Sun: butterfly diagram migration). The short–term light curve is constant, but long-term changes of the mean may take place. Such a *latitudinally* axisymmetric part could explain the changes of the light curve mean during all stages 1–3.
4. Magnetic activity has ceased and the light curve is constant.

6. Conclusions

The "veil" of interference hides the real light curves of chromospherically stars. Here, we show how to look behind this veil and see the two real $f_1(\phi_{\rm act})$ and $f_2(\phi_{\rm rot})$ light curves. These real light curves are less ephemeral than the directly observable light curves of chromospherically active stars that we have been staring at for the past 70 years (Kron 1947). Rarely, once or twice during every lap cycle $P_{\rm cyc} = 4.^{\rm y}43$, the interference of these two curves causes "flip–flop" events in FK Com. The presence or absence of longitudinally nonstationary and stationary parts in the light curves of chromospherically active stars is probably connected to the stages of their magnetic field evolution, as these stars are gradually losing their angular momentum.

Acknowledgements. We thank T. Hackman for his comments of this research. This work has made use of NASA's Astrophysics Data System (ADS) services.

References

Bopp, B. W. & Stencel, R. E. 1981, ApJ, 247, L131
Chugainov, P. F. 1966, Information Bulletin on Variable Stars, 172
Eker, Z., Ak, N. F., Bilir, S., et al. 2008, MNRAS, 389, 1722
Hackman, T., Pelt, J., Mantere, M. J., et al. 2013, A&A, 553, A40
Hale, G. E. 1908, ApJ, 28, 315
Jetsu, L. 1996, A&A, 314, 153
Jetsu, L., Henry, G. W., & Lehtinen, J. 2016, ArXiv e-prints
Jetsu, L. & Pelt, J. 1996, A&AS, 118, 587
Jetsu, L. & Pelt, J. 1999, A&AS, 139, 629
Jetsu, L., Pelt, J., & Tuominen, I. 1993, A&A, 278, 449
Jetsu, L., Pelt, J., & Tuominen, I. 1999, A&A, 351, 212
Korhonen, H., Berdyugina, S. V., & Tuominen, I. 2002, A&A, 390, 179
Kron, G. E. 1947, PASP, 59, 261
Lehtinen, J., Jetsu, L., Hackman, T., Kajatkari, P., & Henry, G. W. 2011, A&A, 527, A136
Lehtinen, J., Jetsu, L., Hackman, T., Kajatkari, P., & Henry, G. W. 2012, A&A, 542, A38
Lehtinen, J., Jetsu, L., Hackman, T., Kajatkari, P., & Henry, G. W. 2016, A&A, 588, A38
Oláh, K., Korhonen, H., Kővári, Z., Forgács-Dajka, E., & Strassmeier, K. G. 2006, A&A, 452, 303
Panov, K. & Dimitrov, D. 2007, A&A, 467, 229
Scargle, J. D. 1982, ApJ, 263, 835
Schwabe, M. 1844, Astronomische Nachrichten, 21, 233
Strassmeier, K. G. 2009, A&A Rev., 17, 251
Strassmeier, K. G. & Rice, J. B. 1998, A&A, 330, 685
Webbink, R. F. 1976, ApJ, 209, 829